Biotemplated hierarchical surfaces and the role of dual length scales on the repellency of impacting droplets

Matthew McCarthy, Konstantinos Gerasopoulos, Ryan Enright, James N. Culver, Reza Ghodssi et al.

Citation: Appl. Phys. Lett. **100**, 263701 (2012); doi: 10.1063/1.4729935
View online: http://dx.doi.org/10.1063/1.4729935
View Table of Contents: http://apl.aip.org/resource/1/APPLAB/v100/i26
Published by the American Institute of Physics.

Biotemplated hierarchical surfaces and the role of dual length scales on the repellency of impacting droplets

Matthew McCarthy,[1,a)] Konstantinos Gerasopoulos,[2] Ryan Enright,[3,4] James N. Culver,[5] Reza Ghodssi,[2] and Evelyn N. Wang[4,b)]
[1]*Department of Mechanical Engineering and Mechanics, Drexel University, Philadelphia, Pennsylvania 19104, USA*
[2]*Department of Material Science and Engineering and Department of Electrical and Computer Engineering, University of Maryland, College Park, Maryland 20742, USA*
[3]*Stokes Institute, University of Limerick, Limerick, Ireland*
[4]*Department of Mechanical Engineering, Massachusetts Institute of Technology, Cambridge, Massachusetts 02139, USA*
[5]*Instititute for Bioscience and Biotechnology Research, Department of Plant Science and Landscape Architecture, University of Maryland, College Park, Maryland 20742, USA*

(Received 6 April 2012; accepted 3 June 2012; published online 28 June 2012)

We fabricated biomimetic hierarchical superhydrophobic surfaces using the *Tobacco mosaic virus* and investigated the role of each length scale during droplet impact by decomposing the micro and nanoscale components. We found that 10 μl water droplets rebounded at impact velocities greater than 4.3 m/s on the hierarchical surfaces, outperforming the nanostructured surfaces, which underwent an observable wetting transition at an impact velocity of 2.7 m/s. This finding demonstrates that each length scale plays a distinct, but complementary, role in maximizing water repellency during droplet impact and, thus, provides insight into the evolutionary development of highly water-repellant hierarchical plant leaves. © *2012 American Institute of Physics*. [http://dx.doi.org/10.1063/1.4729935]

Superhydrophobic surfaces have received widespread attention in the past few decades for applications including self-cleaning,[1] drag reduction,[2] and dew resistance.[3] In particular, significant efforts have been focused on engineering surfaces that mimic the superior non-wetting properties of superhydrophobic wetland and aquatic plant leaves,[1,4,5] which are composed of a hierarchy of micro and nanoscale features. Such hierarchical surfaces exhibit self-cleaning properties and resist wetting upon persistent rainfall. Because of the abundance of water, these wetland plants do not rely on the intake of moisture through their leaves to hydrate. In fact, their superhydrophobic properties are a necessity for survival. Shedding water from the surface dramatically increases the uptake of CO_2 for photosynthesis, and these self-cleaning abilities limit the growth of bacteria and fungi that would otherwise thrive in such hot moist climates.[4,6] Figures 1(a)–1(e) show scanning electron micrographs of three, genetically unrelated, plant leaves that are composed of microscale convex cellular protrusions coated with highly textured waxy nanostructures. Similar hierarchical structures are present on water-repellent plant leaves found across the globe that reside in similar biomes.[6,7]

While surfaces mimicking these plant structures have been fabricated using various techniques including molding,[5,8,9] etching,[9,10] deposition,[5] and growth,[11] past research indicates that nanoscale features alone can achieve similar static contact angles and contact angle hysteresis in comparison to hierarchical surfaces.[5,12,13] These observations raise the question as to why a multitude of genetically dissimilar superhydrophobic plant leaves have independently evolved to contain both nanoscale and microscale surface structures. In this work, we used a biotemplating nanofabrication technique to show that the micro and nanoscale features play distinct, but complementary roles in maximizing the water-repellency of superhydrophobic surfaces during droplet impact. To study these effects we fabricated biomimetic hierarchical surfaces (Figs. 1(f)–1(h)) using the self-assembly and functionalization of the *Tobacco mosaic virus* (TMV)[14–16] onto microfabricated pillars as shown in Fig. 1(i) (see supplemental material for fabrication details[33]).

Figure 2 shows the six surfaces fabricated for the study. The advancing and receding contact angles of flat surfaces both with (Fig. 2(d)) and without (Fig. 2(a)) viral nanostructures, as well as microstructured (Figs. 2(b) and 2(c)) and hierarchical (Figs. 2(e) and 2(f)) surfaces with two different microstructure solid fractions, were experimentally characterized. The microstructure solid fraction of a surface is defined as $S = \pi d^2/4L^2$, where d and L are the pillar diameter and center-to-center spacing, respectively. Figure 2(g) shows the resulting equilibrium contact angle (θ_e) and the contact angle hysteresis (θ_h) for each sample. The nanoscale and hierarchical surfaces both show static contact angles of approximately 170° and contact angle hysteresis values of less than 2° (roll-off tilt angles $<0.25°$). These results highlight the fact that hierarchical geometries characteristic of a number of wetland plant leaves have a negligible effect on the wetting of static droplets and, therefore, cannot reasonably explain the presence of two distinct geometric length scales.

The role of each length scale became evident by studying the dynamics of droplet impact. Droplets typically in the

[a)]M. McCarthy was at the Department of Mechanical Engineering, Massachusetts Institute of Technology, Cambridge, Massachusetts 02139, USA while this research was performed.
[b)]Author to whom correspondence should be addressed. Electronic mail: enwang@mit.edu.

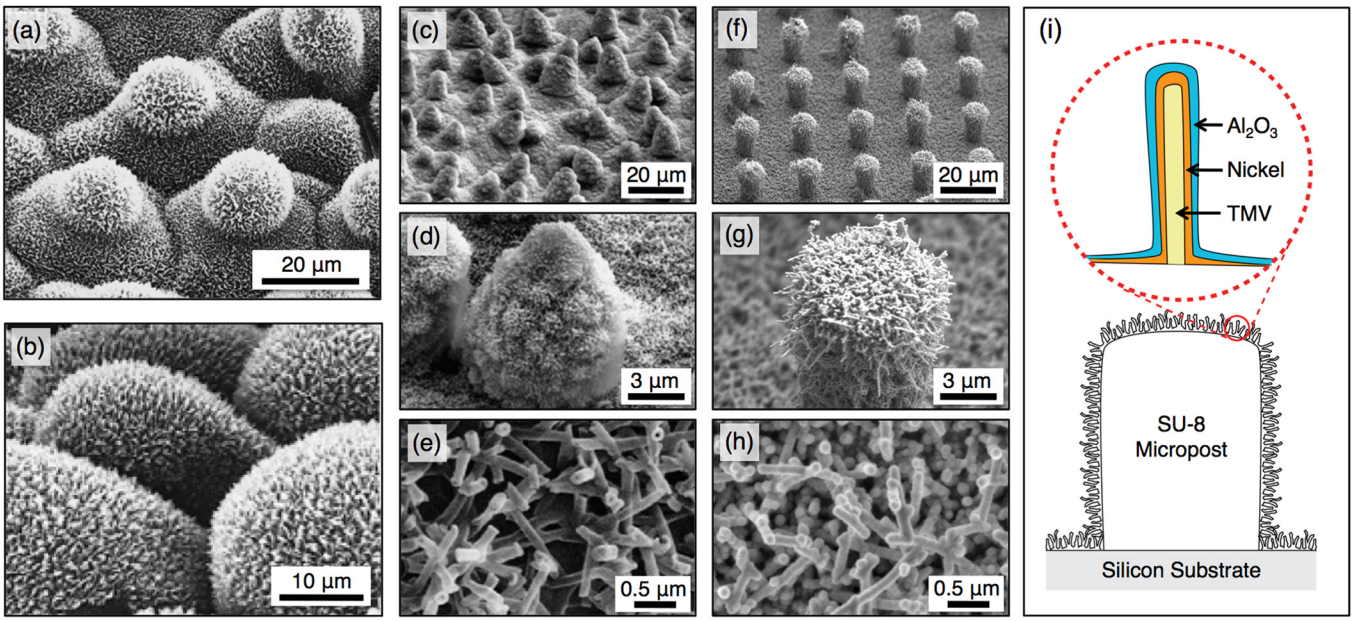

FIG. 1. Superhydrophobic hierarchical plant structures compared to virus-templated biomimetic surfaces. SEM images of the (a) taro plant (*Colocasia esculenta*), (b) parrot feather plant (*Myriophyllum aquaticum*), and (c)–(e) lotus plant (*Nelumbo nucifera*) at various scales (see Refs. 4 and 6). (f)–(h) SEM images of the biomimetic hierarchical structures synthesized for this work using the *Tobacco mosaic virus* assembled onto an array of micropillars at various scales. (a) Reprinted with permission from IOP, Copyright 2007. (b)–(e) Reprinted with permission from Elsevier, Copyright 2009.

non-wetting Cassie state[17] under static conditions can be forced into the wetted Wenzel state[18] by overcoming an energy barrier during impact.[1,19] Previous research has examined the wetting transition of various microstructured,[20,21] nanostructured,[22,23] and hierarchical[9,24] surfaces. This work, however, spans the range of droplet velocities necessary to demonstrate the superior water repellency of hierarchical surfaces in comparison to nanostructured surfaces. Furthermore, this nanofabrication technique offers a simple and flexible method to decompose the hierarchical structures into their nano and micro scale components without compromising size, shape, orientation, and/or coverage. The low temperature process can coat various microstructured surfaces, which is in contrast to other techniques in which both length scales are simultaneously fabricated[11] or an inherent directionality results in non-uniform nanostructured coatings.[8,9]

Each of the fabricated surface types was subjected to the impact of 10 μl droplets (diameter, $D = 2.7$ mm) at speeds ranging from 0.2–4.3 m/s, corresponding to droplet Reynolds numbers and Weber numbers (defined using the droplet diameter and impact velocity) ranging from Re = 540–11,610 and We = 1.5–826, respectively. Figures 3(a) and 3(b) show high-speed images of water droplets impacting microstructured ($S = 0.38$) and nanostructured surfaces above their critical velocities, where wetting was observed for both. Note that, in the present context, we define "wetting" as an observable Cassie-to-Wenzel transition during droplet impact. A large pinned droplet ($D \sim 1.8$ mm) remained on the microstructured surface at a velocity of 2.1 m/s, and a small pinned droplet ($D \sim 0.6$ mm) remained on the nanostructured surface for a velocity of 4.3 m/s. Yet at the same velocity of 4.3 m/s, the hierarchical surface (Fig. 3(c)) showed no indication of wetting. Splashing and break-up into smaller satellite droplets was observed for both the nanostructured and hierarchically structured surfaces for We ~ 150.

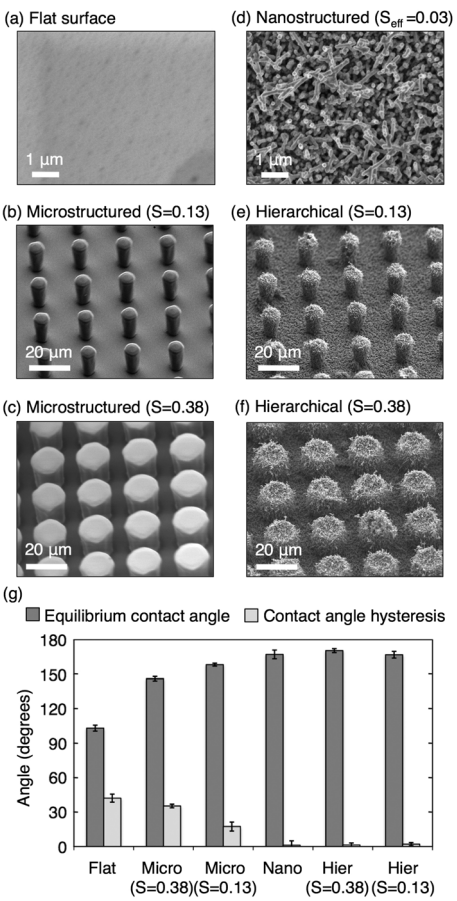

FIG. 2. Wetting on microstructured, nanostructured, and hierarchical surfaces. SEM images of experimentally characterized surfaces: (a) a flat surface, (b), (c) microstructured surfaces with 15 μm tall pillars spaced 20 μm apart with diameters and microstructure solid fractions of (b) $d = 8$ μm, $S = 0.13$ and (c) $d = 14$ μm, $S = 0.38$, (d) the nanostructured surface with $d = 80$ nm and $S_{eff} = 0.03$, and (e), (f) hierarchical surfaces with 15 μm tall micropillars spaced 20 μm apart with diameters and microstructure solid fractions of (e) $d = 8$ μm, $S = 0.13$ and (f) $d = 14$ μm, $S = 0.38$. (g) Equilibrium contact angle and contact angle hysteresis measured on the surfaces shown in (a)–(f).

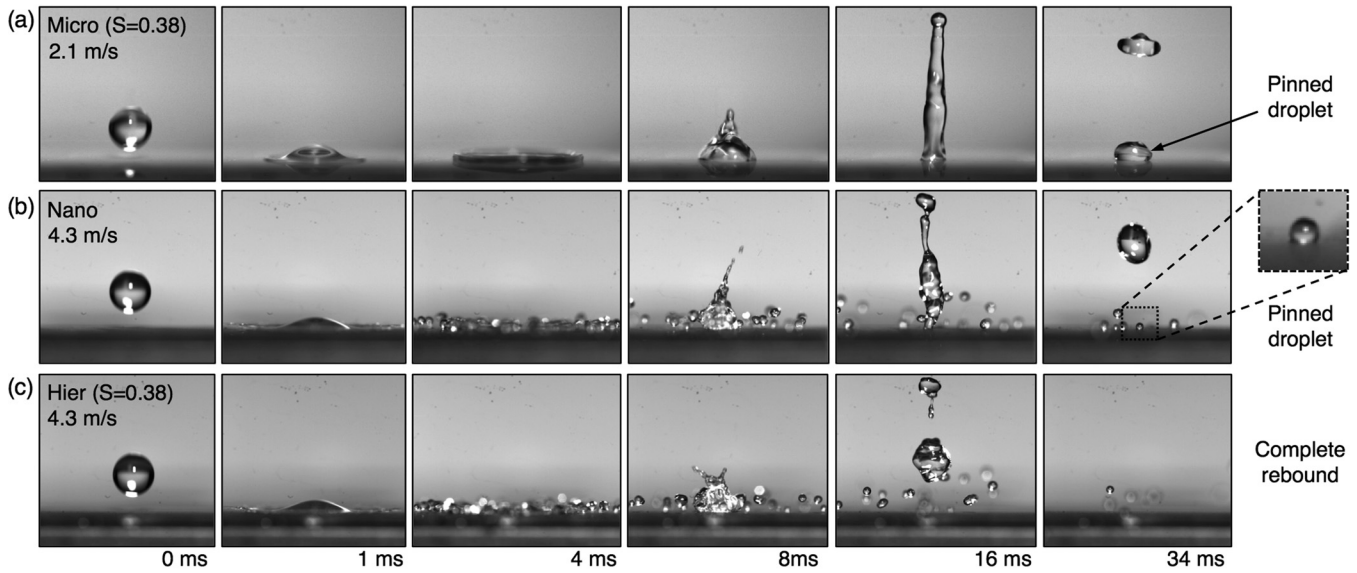

FIG. 3. High-speed imaging of droplet impact on structured surfaces with 10 μL droplets ($D \sim 2.7$ mm) impacting the (a) microstructured surface ($S = 0.38$) with a velocity of 2.1 m/s, showing a large portion of the droplet wetted to the surface and partial rebound (pinned diameter ~1.8 mm), (b) nanostructured surface with a velocity of 4.3 m/s showing partial wetting and break-up into satellite droplets (pinned diameter ~0.6 mm), and (c) hierarchical surface ($S = 0.38$) with a velocity of 4.3 m/s showing complete rebound and break-up into satellite droplets.

Figure 4 shows the critical impact velocities, V^*, at which wetting of each structured surface was first observed. The criterion for wetting was defined by the minimum pinned drop size resolved by the high-speed imaging system (~100 μm). For speeds higher than V^*, the droplet (or some fraction of the droplet) remains pinned to the surface indicating a transition to the Wenzel state in that region. Using deionized (DI) water droplets, the microstructured surfaces wet at relatively low critical velocities <0.2 m/s and 1.4 m/s for the $S = 0.13$ and $S = 0.38$ surfaces, respectively, while the nanostructured surface transitioned to a wetted state at 2.7 m/s (see movies in supplementary material[33]).

The critical velocities for the hierarchical surfaces were not determined using DI water due to the maximum speed achievable with the experimental apparatus (limited by the maximum drop height), but exceeded $V = 4.3$ m/s. Accordingly, an aqueous mixture with 2 wt. % isopropyl alcohol was used to lower the surface tension to $\gamma = 60.4 \pm 0.55$ mN/m,[25]

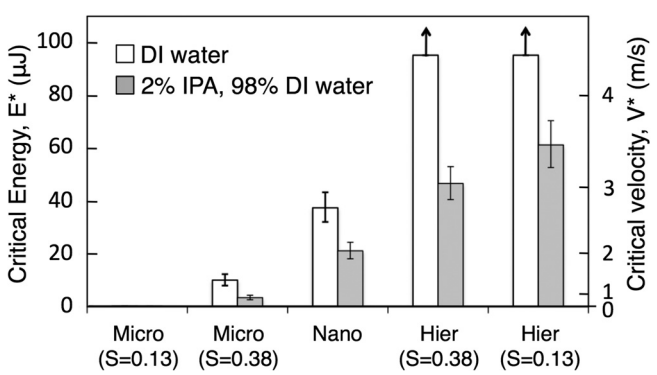

FIG. 4. Droplet impact experimental results showing the critical kinetic energy, $E^* = (1/2)mV^{*2}$, where m is the droplet mass, and critical velocity, V^*, required to wet each surface for DI water and the water-alcohol mixture. The critical values for pure water to wet the hierarchical surfaces exceeded the capabilities of the apparatus; the upward arrows in the graph denote this.

resulting in an equilibrium droplet contact angle of $\theta_e \approx 96.5° \pm 3.6°$ with a hysteresis of $\theta_h = 43.6° \pm 5.5°$ on a corresponding smooth, silanated surface. The critical velocities for DI water and the water-alcohol mixture along with the associated critical kinetic energies of the droplets are shown in Fig. 4. For both liquids, the critical velocities and critical kinetic energies required to wet the hierarchical surfaces were at least ~1.5 times and 2–3 times larger, respectively, than that of the nanostructures alone.

For a droplet to transition to a wetted state, it must overcome an energy barrier between the suspended Cassie state and the pinned Wenzel state. This energy barrier was defined by the anti-wetting capillary pressure of the smallest length-scale structure present on the surface. Therefore, the energy barrier for the nanostructured and hierarchically structured surfaces should be identical.

Figure 5 shows the critical dynamic pressure, $P_d^* = 0.5\rho V^{*2}$, where ρ is the density of the droplet, scaled by the "sliding mode" anti-wetting capillary pressure, $P_c = 4S\gamma\cos\theta_a/d(S\text{-}1)$, where θ_a is the advancing contact angle,[25] as opposed to the "touch down" mode[26,27] (see supplementary material[33]). For the case of the hierarchical surfaces, the capillary pressure associated with the nanostructure (i.e., the smallest length scale) was used to define the P_d^*/P_c ratio. To estimate P_c for the nanostructures, we extracted an effective solid fraction, $S_{eff} = 0.03$ from the measured apparent equilibrium contact angle (Fig. 2) *via* the Cassie-Baxter equation.[17]

On the samples where wetting transition could be observed, the critical dynamic pressure was at least one order of magnitude smaller than the capillary pressure, $P_d^*/P_c \sim 0.01$–0.1. This commonly observed result is attributed to the water hammer effect where large compressible pressures are generated upon impact.[21,22] Yet, in the case of the hierarchical surfaces, the ratio is more than double that of the nanostructures alone. These results suggest that the

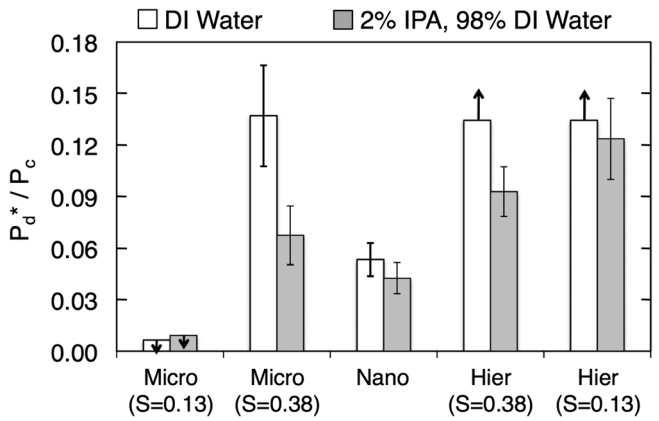

FIG. 5. Critical dynamic pressure scaled by the calculated capillary pressure, P_d^*/P_c, for DI water and the water-alcohol mixture. For both the nanostructured and hierarchical samples P_c is defined using the capillary pressure of the nanoscale structures.

microstructural component of the hierarchical surfaces plays a dissipative role that extends the observable wetting transition to impact velocities significantly higher than that of the nanostructure alone. While the inclusion of microstructural component had no discernible effect on the static wetting behavior, it significantly increased the ability of structured surface to withstand transition to a wetted state and repel water droplets during impact.

To explain the role of the microstructure features of the hierarchical surfaces, the nature of the water hammer pressure needs to be considered. During the initial impact of a spherical droplet onto a flat surface, the three-phase contact line between air, water, and the surface is traveling faster than the speed of sound in the liquid leading to compression in the stagnation region.[28,29] The resulting pressure, $P_{WH} \sim \rho CV$, where C is the speed of sound and V is the impact velocity, can be up to two orders of magnitude larger than the associated incompressible dynamic pressure, P_d.[28,29] After the three-phase contact line slows below the sonic limit, shock waves overtake the contact line and the fluid jets outwards. The diameter of the compressible region, X, at which the contact line slows to below sonic conditions for a spherical droplet impacting a flat surface is[28,29]

$$X = \frac{DV}{C}. \tag{1}$$

Naturally occurring raindrops, with diameters, D, of 1–4 mm and terminal velocities of 4–9 m/s,[30,31] impacting flat surfaces will generate compressible regions with diameters, X, of 2–24 μm. Interestingly, this range of diameters closely matches the length scale of the microstructures found on hierarchical water repellent plant leaves (Figs. 1(a)–1(e)) and suggests that the addition of surface topology with length scales on the order of the compressible region impedes the development and/or propagation of the pressures generated in the stagnation region.

Qualitatively, we envision the following sequence of events for droplet impact on the hierarchical surfaces. Upon initial droplet impact, the compressible no-flow regions are formed at the tops of the microstructure component. Subsequently, the liquid can expand from these regions of large compression into the space between the microstructures providing an efficient mechanism to release this pressure and limit the plan area of the sample experiencing large water hammer pressures. The nanostructure component will easily wet within the shock region since $P_{WH}/P_c \sim 100$. However, the nanostructures outside of the shock region, where the pressure tends toward P_d, remain unwetted since $P_c \gg P_d$. Furthermore, the negligible contact angle hysteresis associated with the nanostructures in the unwetted state allows the liquid between the larger scale microstructure of the hierarchical surface to be expelled, unlike the case of the microstructures alone, such that the droplet is free to de-wet back to the region of the small shock zone during recoil. Collectively, these effects lead to a substantial increase in wetting robustness. Indeed, this view of the impact process may explain the apparent increase in robustness demonstrated by the hierarchical surface with the smallest microstructure solid fraction (see Figs. 4 and 5) by virtue of the larger volume ($\sim$1.4×) available for liquid re-expansion around each nanostructured micropillar (for the same center-to-center spacing).

While the critical velocities of DI water droplets impacting the hierarchical structures were not found ($V^* > 4.3$ m/s), examining the balance between the critical water hammer pressure and the capillary pressure suggests the following scaling:

$$\frac{V^*_{H_2O}}{\gamma_{H_2O}\cos\theta_{a,H_2O}} \propto \frac{V^*_{IPA+H_2O}}{\gamma_{IPA+H_2O}\cos\theta_{a,IPA+H_2O}}. \tag{2}$$

Considering the results obtained for the water-alcohol mixture, Eq. (2) predicts the critical velocities of the hierarchical structures under water droplet impact to be $\sim$4.3 m/s and $\sim$4.9 m/s for the surfaces with microstructure solid fractions of $S = 0.38$ and $S = 0.13$, respectively. The significance of this result can be appreciated by evaluating the raindrop size distribution during convective rainfall in the West Bengal region of India, a natural habitat of the lotus.[32] We find that approximately 70%–75% of the total rainfall is below the velocity ($\sim$5 m/s) successfully repelled by the biomimetic hierarchical surfaces studied in this work. For the nanostructures alone, the percentage drops to $\sim$20%. If we now consider the reported intrinsic wettability of the lotus wax,[5] the scaling given by Eq. (2) predicts a critical impact velocity of $V^* \approx 8.1$ m/s. This result coincides with more than $\sim$95% of falling rain drops being repelled by the lotus leaf, which is consistent with observations of the lotus remaining dry following rainstorms in its natural habitat.

In conclusion, by leveraging a conformal biotemplating nanofabrication technique, we have experimentally demonstrated that the micro and nanoscale components of lotus-like hierarchical superhydrophobic surfaces play distinct, but complementary, roles in repelling wetting by droplet impact. The nanoscale component provides a large anti-wetting capillary pressure, while the microscale component impedes the development and propagation of pressures associated with liquid compression. Thus, this work provides insight into the physical principles leading to the evolution of hierarchical water repellent plant leaves and represents a paradigm shift in the design of robust water repellent superhydrophobic surfaces.

M.M. and E.N.W. acknowledge funding support from DARPA with Dr. Tom Kenny as program manager. R.E. acknowledges funding received from the Irish Research Council for Science, Engineering, and Technology, co-funded by Marie Curie Actions under FP7. The authors also would like to thank Professor John Bush at MIT for helpful discussions.

[1]X. Feng and L. Jiang, Adv. Mater. **18**, 3063 (2006).
[2]J. P. Rothstein, Ann. Rev. Fluid Mech. **42**, 89 (2010).
[3]J. B. Boreyko and C. H. Chen, Phys. Rev. Lett. **103**, 184501 (2009).
[4]A. Solga, Z. Cerman, B. Striffler, M. Spaeth, and W. Barthlott, Bioinsp. and Biomim. **2**, S126 (2007).
[5]K. Koch, B. Bhushan, Y. Jung, and W. Barthlott, Soft Matter **5**, 1386 (2009).
[6]K. Koch, B. Bhushan, and W. Barthlott, Prog. Mater. Sci. **54**, 137 (2009).
[7]K. Koch and W. Barthlott, Philos. Trans. R. Soc. A **367**, 1487 (2009).
[8]H. Jeong, S. Lee, J. Kim, and K. Suh, Langmuir **22**, 1640 (2006).
[9]M. Chen, T. Hsu, Y. Chuang, and F. Tseng, Appl. Phys. Lett. **95**, 023702 (2008).
[10]Y. Kwon, N. Patankar, J. Choi, and J. Lee, Langmuir **25**(11), 6129 (2009).
[11]X. Liu and J. He, Langmuir **25**(19), 11822 (2009).
[12]K. Lau, J. Bico, K. Teo, M. Chhowalla, G. Amaratunga, W. Milne, G. McKinley, and K. Gleason, Nano Lett. **3**, 1701 (2003).
[13]H. Erbil, A. Demirel, Y. Avci, and O. Mert, Science **299**, 1377 (2003).
[14]E. Royston, A. Ghosh, P. Kofinas, M. Harris, and J. Culver, Langmuir **24**, 906 (2008).
[15]K. Gerasopoulos, M. McCarthy, E. Royston, J. Culver, and R. Ghodssi, J. Micromech. Microeng. **18**(10), 104003 (2008).
[16]K. Gerasopoulos, M. McCarthy, P. Banerjee, X. Fan, J. Culver, and R. Ghodssi, Nanotechnology **21**(5), 055304 (2010).
[17]A. Cassie and S. Baxter, Trans. Faraday Soc. **40**, 546 (1944).
[18]R. Wenzel, Ind. Eng. Chem. **28**, 988 (1936).
[19]A. Lafuma and D. Quere, Nat. Mater. **2**, 457 (2003).
[20]L. Mishchenko, B. Hatton, V. Bahadur, J. Taylor, T. Krupenkin, and J. Aizenberg, ACS Nano **4**(12), 7699 (2011).
[21]M. Reyssat, A. Pépin, F. Marty, Y. Chen, and D. Quéré, Europhys. Lett. **74**(2), 306 (2006).
[22]T. Deng, K. Varanasi, M. Hsu, N. Bhate, C. Keimel, J. Stein, and M. Blohm, Appl. Phys. Lett. **94**, 133109 (2009).
[23]M. Kwon, A. Paxson, K. Varanasi, and N. Patankar, Phys. Rev. Lett. **106**, 036102 (2011).
[24]Y. Jung and B. Bhushan, Langmuir **25**(16), 9208 (2009).
[25]G. Vazquez, E. Alvarez, and J. Navaza, Chem. Eng. Data **40**, 611 (1995).
[26]D. Bartolo, F. Bouamrirene, E. Verneuil, A. Buguin, P. Silberzan, and S. Moulinet, Europhys. Lett. **74**(2), 299 (2006).
[27]E. Lobaton and S. Salamon, J. Colloid Interface Sci. **314**(1), 184 (2007).
[28]O. Engel, J. Appl. Phys. **44**, 692 (1973).
[29]J. Field, Phys. Med. Biol. **36**, 1475 (1991).
[30]K. Beard, J. Atmos. Sci. **33**, 851 (1976).
[31]A. Spilhaus, J. Meteorol. **5**, 108 (1948).
[32]K. Chakravarty and A. Maitra, in *IEEE Applied Electromagnetics Conference (AEMC)*, Kolkata, India, 14–16 December 2009.
[33]See supplementary material at http://dx.doi.org/10.1063/1.4729935 for complete fabrication methods, experimental details, and high speed imaging of droplet impact tests.